

Local Field Potential Journey into the Basal Ganglia

Eitan E. Asher¹, Maya Slovik^{2,3}, Rae Mitelman^{2,3}, Hagai Bergman^{2,3}, Shlomo Havlin¹, Shay Moshel^{1,2,3,4}

¹Department of Physics, Bar-Ilan University, Ramat Gan, Israel

²Department of Medical Neurobiology, The Hebrew University-Hadassah Medical School, Jerusalem, Israel

³ The Edmond and Lily Safra Center for Brain Sciences, The Hebrew University, Jerusalem, Israel

⁴ Nuclear Research Center Negev, Beer-Sheva, Israel

E-mail: shaymoshel@gmail.com

Abstract.

Local field potential (LFP) in the basal ganglia (BG) nuclei in the brain has attracted much research and clinical interest. However, the origin of this signal is still under debate throughout the last decades. The question is whether it is a local sub-threshold phenomenon, e.g., reflecting the synaptic inputs to neurons in the recording area, or it is a flow of electrical signals which are generated from simultaneous firing neurons in the cerebral cortex and obeys the Maxwell equations (volume conduction). In this study, we recorded in Non-human primate (NHP) brain simultaneously LFP's from the cerebral cortex, in the frontal lobe and primary motor cortex (M1), and in multiple sites in BG nuclei: the striatum, globus pallidus and subthalamic nucleus. All the records were taken with the NHPs in quite awake state with no engagement in behavioral task. Developing and applying a novel method to identify significant cross correlations (potential links) while removing "spurious" correlations, we found a tool that may discriminate between the two major phenomena of synaptic inputs (information flow) and volume conduction. We find mainly two major paths flows of BG field potentials, that propagate with two different time delays, from primary motor cortex and from the frontal cortex. Our results indicate that the two paths flows may represent the two mechanisms of volume conduction and information flow.

1. Introduction

Broad band field potential becomes an important and powerful tool to understand many neuronal functions, abnormalities and clinical phenomena. Behavioral studies use local field potential (LFP) activity to describe cognitive occurrences [1–3] and sensory response [4–6]. Brain machine interface tools have been developed based on [7] and electroencephalogram (EEG) signals [8]. Subthalamic nucleus LFPs has been found to be coupled with EEGs related to cortical somatosensory areas [9], and neural discharge rates found to be coupled with LFPs signals in the cerebral cortex during voluntary movements [10]. Brain diseases such as Parkinson disease (PD) and schizophrenia, cause to the increase of brain abnormal oscillations in neuronal signals, as single-unit, multi-unit activity and LFPs in the brain, such as, in the Basal Ganglia (BG) and cerebral cortex [11–13]. LFPs span the frequency ranges of 1-80 Hz or 1-400 Hz, if one includes the high gamma peaks reported at 65-90 Hz and 250-350 Hz [14]. However, [15] shows possible confounding factors in the high frequency regime of LFP, whereas spikes have their maximal power around 1000 Hz. Thus, although LFP oscillations have been thought to imply spike synchronization [12, 16–18], they are more likely to represent sub-threshold phenomena as synaptic inputs [1, 19] which is probably correlated with spike activity. Broadband field potentials have been also found to be correlated with spontaneous cerebral low-frequency blood oxygen level-dependent (BOLD) fluctuations [20, 21]. Hermes et al., [21] described that, the two measures, the BOLD amplitude and electrocortigram (ECoG) (xx-yy Hz) broadband power are correlated in cerebral cortex (V1, V2 and V3), where the BOLD amplitude and alpha power (8–13 Hz) are negatively correlated, and the BOLD amplitude and narrow-band gamma power (30–80 Hz) are uncorrelated. They pointed out that the two measures, nevertheless, provide complementary information about human brain activity, and they infer that features of the field potential that are uncorrelated with BOLD arise largely from changes in neuronal synchrony, rather than, level of direct neuronal activity. Although it is found that broadband field potential plays a key role for analyzing brain behavior and it is easy to record, the origin of the local field potential (LFP) remains under debate. Many studies suggest that this signal carries valuable neuronal information as the local synaptic inputs [xx]. In spite of these, there are studies that describe these signals as propagative electromagnetic waves behave as a volume conductance, obeying the Maxwell equations[xx]. An intermediate studies suggest that these signals have mixed characters of both volume conduction and a summation of the extracellular fields [1]. Parabucki et al [22] described a strong LFP signals coupling between the cerebral cortex, during whisker stimulation in a mice, with a dissected part of the olfactory bulb. They recorded simultaneously the cerebral cortex and the dissected part, and describe that the LFP “passed” from the cortex through the dissected part as a volume conducted signal. However, in spite of these remarkable studies, to date we still do not have a clear picture for describing the activity of broadband field potentials, whether it is a volume conducted electromagnetic waves that spreads inside the deep layers in the brain or they carry a valuable information as synaptic inputs. In order to explore this issue, we map LFP signals from

the cerebral cortex through the basal ganglia nuclei, where we recorded simultaneously the signals from the cerebral cortex and signals in the deep layers of the basal ganglia (BG) nuclei, of human primate model during wake. Using micro-electrodes, we recorded the full electrophysiological signal (row-data) in the range of [1, 6000] Hz, with 1-7 electrodes which were fixed in the 5th cortex layer (pyramidal cells) for all recording session, see Fig.1(a). One electrode that has been moved towards to the BG nuclei and has been simultaneously recorded every 200 μm , for a duration of 120 seconds, since the entrance to the cerebral cortex (frontal lobe) and passed through: cortex, striatum, globus pallidus (external - GPe, internal - GPi), internal capsule and the subthalamic nucleus. To get LFP signal we filtered the full signal (raw data) to 0.1-80Hz and analyzed the relationship between neuronal activity in the cerebral cortex and the deep BG brain layers.

2. Methods

2.1. Animals, surgery and MRI

We conducted the experiments on one African Green monkey (*Cercopithecus aethiops*, females, weighing between 3.3 and 4.4 Kg). All procedures were conducted in accordance with the Hebrew University guidelines for animal care and the National Institute of Health Guide for the Care and Use of Laboratory Animals. The Hebrew University is an AAALAC (Association for Assessment and Accreditation of Laboratory Animal Care) approved institute. The monkey was trained to sit quietly in a primate chair. After training, the animal underwent a surgical implantation of a Cylux MRI compatible 27*27 mm recording chamber (Alpha-Omega, Israel) and head holder (Crist Instruments, MD). The location of the chamber was determined by a primate stereotaxic atlas (Contreras et al. 1981; Martin et al. 2000) to be above the right primary motor cortex (M1), globus pallidus (Gp) and the subthalamic nucleus (Stn). A few days after surgery, an MRI scan was performed to determine its exact stereotaxic location.

2.2. Recording and data acquisition

During recording sessions, the animals were seated in a primate chair with their head and hands restrained, but were free to move their trunk and legs. All recording were done during quite alert state. The verification of recording location was carried out separately for the target structures, the cerebral cortex and the deep nuclei of the basal ganglia (BG) complex: striatum, globus pallidus and the subthalamic nucleus. Extra cellular data domain was amplified with a gain of 5K, band-pass filtered with a 1-6000 Hz four-pole hardware Butterworth filter and continuously sampled at 25 kHz.

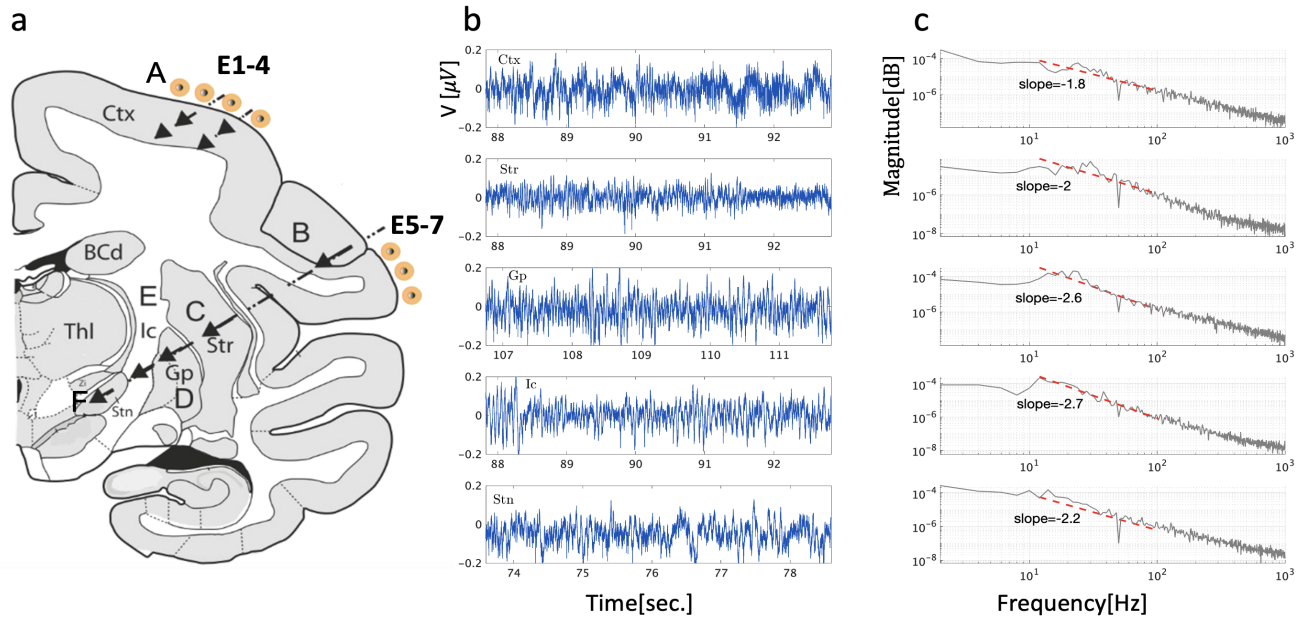


Figure 1: Hemi-coronal illustration from Macaque AC atlas - 6 mm and electrodes setup, raw data and power spectrum densities. (a) We place 7 electrodes in the cerebral cortex, fixed on the 5th layer of pyramidal cells. Electrodes 1-4 (E1-4) were permanently located on the right-hemisphere, primary M1-motor-cortex, and electrodes 5-7 (E5-7) on the right hemisphere - frontal cortex. One electrode aimed to the basal ganglia, moving to the deepest layers of the basal ganglia passing through the recording sites in: the cerebral cortex (Ctx), striatum (Str), globus pallidus (Gp) internal capsule (Ic) and subthalamic nucleus (Stn). We start the recording in the entrance of the nucleus surface as been detected according to a typical electrophysiological activity. Each site has been recorded for time duration of 120 seconds. After completing the recording, we move in a step of 200 micrometer deeper, as illustrated by the arrows. (labels in cartoon: A to F mark the recorded nucleus). (b) Examples of 5 seconds records of raw local field potential data as recorded from the nucleus that were analyzed, from shallow to deep: Ctx, Str, Gp, Ic and Stn, and (c) their power spectral density, after applying a band-pass filter to remove the 50Hz band.

The data has been stored by a data acquisition system (Alpha-Map, Alpha-Omega, Israel) for offline analysis. The animals' behavior has been monitored by a computerized video surveillance system (monkeys F and Su: GV-650, GeoVision, Taiwan; monkeys F and Su: GV-2400, GeoVision, Taiwan) connected to four infrared digital cameras. We used two arrays of four glass-coated tungsten microelectrodes (impedance measured at 1 kHz, range 0.2-0.6 MOhm), confined within a cylindrical metal guide (1.36 mm internal diameter). The electrodes were positioned (E1-4 electrodes) in the area of the primary motor cortex and the other E5-7 electrodes were fixed at frontal cortex 5th layer and aimed to the basal ganglia nuclei, see Fig.1(a). This was done using the double Microdriving Terminal and Electrode Positioning System (Double MT and EPS, Alpha-Omega, Israel), that allows independent movement of each electrode. During the recording procedure, we fixed E1-7 electrodes at the 5th layer of the cerebral cortex (M1 and the frontal

Location	E1-7-Ctx	E1-7-Str	E1-7-Gp	E1-7-Ic	E1-7-Stn
Sites	210	219	91	20	18
Pairs	1318	1331	561	140	126

Table 1: **Database of the study.** Number of recorded sites of each nucleus, and number of total cortex electrode-deep electrode pairs. The deep electrode was moved in $200\mu\text{m}$ steps from the cortex towards the BG. Each location that has been visited is a site. At each site, the signal that was recorded from the deep electrode has been analyzed using cross correlation against its matching time record of the E1-7 electrodes, resulting in the number of total pairs, given in the Table.

cortex above the BG) and a moving 8th electrode, has been advanced towards the BG nuclei (Figure 1A). We started simultaneous recordings of the Ctx electrodes (E1-7) when the moving electrode entered the cerebral cortex. We recorded at each location for time duration of two minutes, after waiting several seconds for stabilization. When we completed the specific site recording; we moved further the traveling electrode by $200\ \mu\text{m}$ to the next deeper location. The verification of recording location was carried out separately for the target structures, using their typical electrophysiological signatures (Moshel et al., 2013). In our data analysis we utilized Python 3.6 and custom-made MATLAB19a (R2019a) routines. Our database contains 13 trajectories from the basal ganglia nuclei. Data records are summed in Table 1.

2.3. Cross-correlation and surrogate analysis to identify significant interactions

In order to quantify the interaction represented by similarity between two signals in both sites X and Y. (One site is always the site from the deep electrode, and the other one is taken from the electrodes that are located on the cortex (electrodes E1-7), see Fig.1. To this end, we analyze similarity, using cross correlation, between the of two simultaneous signals x and y each of length N . We divide both signals x and y into N_L -overlapping segments ν of equal length $L=2.5$ s. We choose an overlap of $L/4=0.625$ s. Thus, for each 120 second record we get $N_L = 63$ time windows. Before the analysis, the signal in each segment ν is subtracted by its mean, in order to remove constant trends in the data. This normalization assures that the coupling between the signals x and y is not affected by their relative amplitudes, but mainly on variations from average.. Next, we calculate the cross correlation function, $R_{xy}^\nu(\tau) = \sum_{\tau=-n/2}^{n/2} x^\nu(n + \tau) * y^\nu(n)$ within each segment $\nu = 1, \dots, N_L$. We then normalize the sequence so that the auto-correlations at zero lag equals 1: $\hat{R}(\tau) = \frac{1}{\sqrt{\hat{R}_{xx}(0)\hat{R}_{yy}(0)}}\hat{R}_{xy}(\tau)$ for each window ν . In order to distinguish between significant and non-significant interactions between signals x and y , we study how their cross-correlation R decays when shifting the signals against each other. The more it decays the more significant are the links. Panels (e) and (f) in Fig. (2) show examples of R versus time shift τ and suggest that more synchronized signals (with higher R values) have a marked decay of $R(\tau)$ (panel (e)) that may not be seen for less synchronized signals (panel (f)). To better quantify this observation, we define a

significance value w (standard score) that normalizes the maximum cross correlation index R_{max} (detected at a particular time shift τ^*) by the “background noise” characterized by the mean and standard deviation of $R(\tau)$. Colloquially, w gives an estimate of how much R_{max} “stands out” from the background. Specifically, how many standard deviations the value of the peak is farther from the noise. That is,

$$w^{i,j} = \frac{(|R_{max}|) - \langle R \rangle}{\sigma(R)} \quad (1)$$

where $\langle R(\tau) \rangle$ ($\sigma(R(\tau))$) is the mean (standard deviation) of $R(\tau)$. From Eq. (1) one can see that if R_{max} is much larger than the background, w is higher, indicating a more significant coupling between signals x and y . On the other hand, if R_{max} does not stand out from the $R(\tau)$ background, w is lower and implies non significant x - y interaction. Figure (2)g) shows results obtained from 10,000 pairs of signals, where each pair of signals is either taken at the same time (simultaneously, real” data) or at different times (“surrogate” data). It can be seen from the figure that high w values for the real data are usually detected for small shifts τ^* (of the order of few tens of milliseconds), which is consistent with the fact that brain waves generally propagate rather quickly [23, 24]. Combining the two conditions, we consider x - y interactions as significant only if $\tau^* \in [-0.05, 0.05]$ seconds and $w > 4.5$.

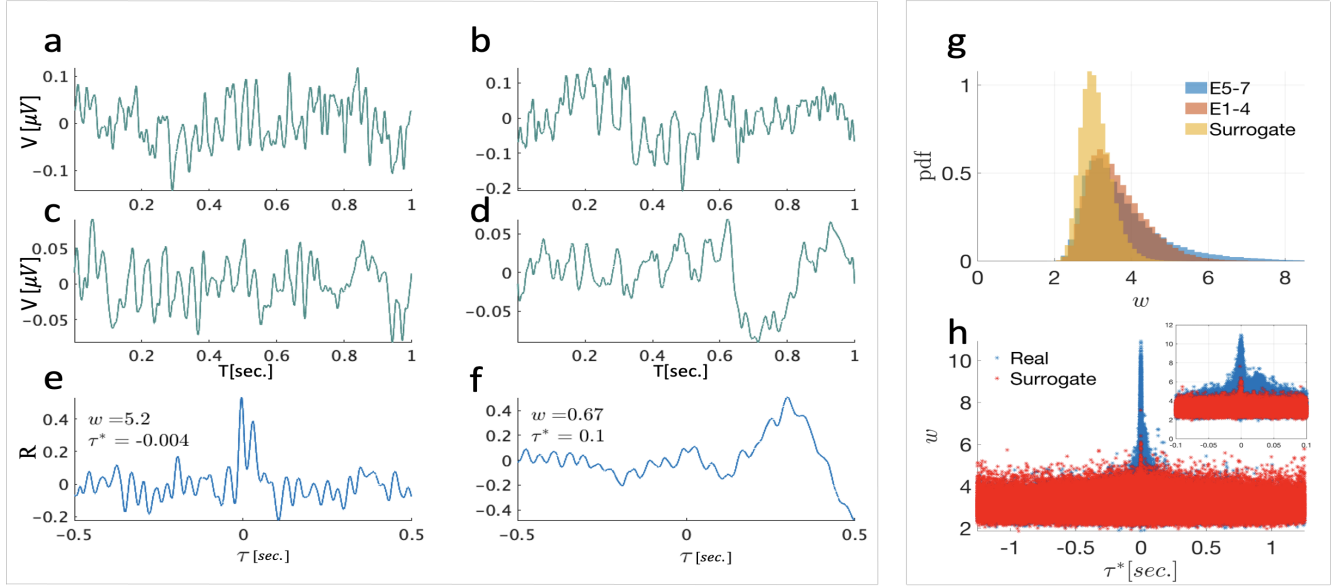


Figure 2: Correlations and surrogate analysis for identifying significant interactions. (a-f) Demonstration of two pairs of signals (blue curves in (a)-(c) and (b)-(d)) obtained simultaneously from different nuclei after applying a [0-80Hz] low-pass-filter to the raw LFP data. (e) and (f) The cross correlation index R as a function of the shift τ between the signals (a) vs. (c) and (b) vs. (d), respectively. The signals from (a) and (c) yield a marked maximum R at shift $\tau^* = \tau|_{R(\tau) \equiv R_{\max}} = 0$, and $R(\tau)$ decays rapidly for $|\tau| > 0$. (b) and (d) demonstrate uncorrelated signals, since, $R(\tau)$ in (f) shows fluctuating behavior without clear decay, i.e., uncorrelated signals. A significance value w characterizes $R(\tau)$ by normalizing R_{\max} by the mean and standard deviation of $R(\tau)$ (Eq. 1). Correspondingly, we obtain a higher w value for panel (e) ($w = 5.2$) than for panel (f) ($w = .67$). (g) distribution of w for all data, taken from electrodes and E5-7, compared to surrogate signals. For the real data, we show w for all time windows that were analyzed. Surrogate signals are signals that were randomly chosen from different electrodes, different nucleus, and also at different times. Note that the E5-7 (frontal-lobe) electrodes, the distribution of real w 's is higher, Compared to those of the ones were fixed at cortex M1 , electrodes E1-4, which means that Lfps from frontal lobe are more correlated. Surrogate signals yield w values distribution that is significantly lower than w 's of real signals; maximum w value for surrogate signals is around 4. Panel (h) shows that highest w values are observed for $\tau^* \approx 0$. In this scatter plot we show 5000 samples of w vs. τ^* for real data (blue circles) and surrogate data (red dots). Real signals are taken at the same time, comparing deep and Ctx signals, whereas surrogate pairs were chosen randomly from different times. Clearly, higher w values are obtained for real signals for $\tau^* \approx 0$. In contrast, surrogate analysis does not lead to higher w values around $\tau^* \approx 0$ and shows a uniform w vs. τ^* distribution.

3. Results

Correlations, weights and τ^* distributions. We find that there exist strong correlations between Ctx-Ctx, Ctx-Str, Ctx-Gp, Ctx-Ic and Ctx-Stn, see Fig. 11. We define the time lag τ^* at which $C(\tau)$ is maximal, as the time delay of pairs x and y . Whether τ is positive or negative, determines the

location in which the signal was detected first. We find that when looking on real links in which $w > 4.5$, the $\langle \tau^* \rangle$ is around factor two larger for the electrodes located at primary motor cortex - M1 (E1-4) than the ones located at frontal cortex E5-7, see Fig. 4 (a). Additionally, when plotting the distributions of τ^* for all possible interactions, the distribution of E1-4 electrodes is much wider than E5-7.

Link lifetime. Another question of interest is what is the time duration or "lifetime" of a link? As before, we divide each recording time period at each site (120 s) into 2.5 s overlapping windows, with a fraction of 0.25 window length overlap. Then, by calculating the cross-correlation of the signal of a given site with its simultaneous time signal in the cortex electrode, we find the link strength w by applying Eq.1. If $w > 4.5$, we regard the two signals as linked. Then, we find the time duration (how many successive windows are correlated) of those links, and plot their distribution for all the nuclei interactions that were probed. The results are presented in Fig.5. We find that, as the interaction involves towards deeper nucleus, there is a clear decrease in the link length.

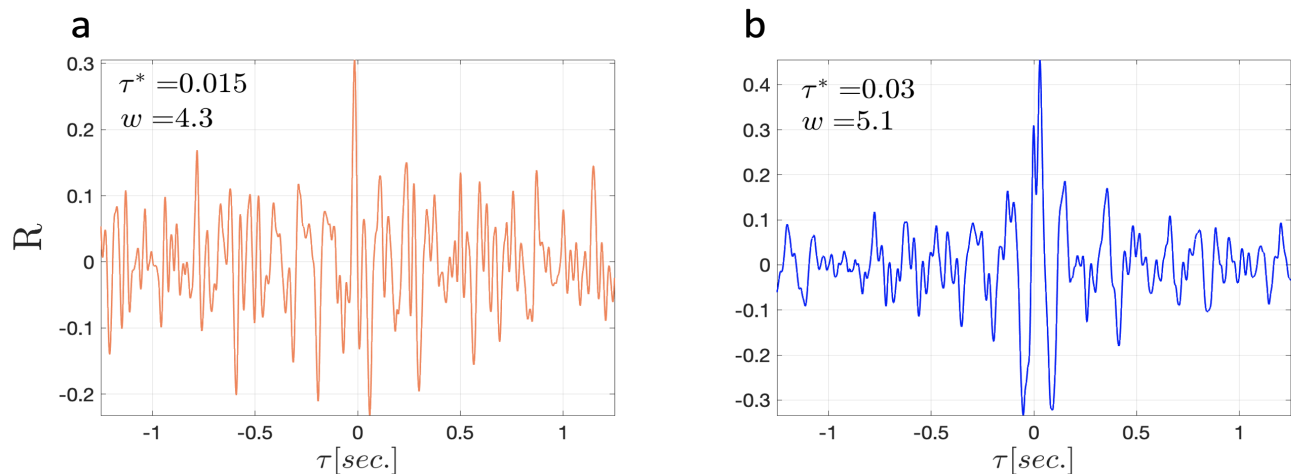


Figure 3: **Cross-correlation examples.** **a.** A cross-correlation result of two signals, one is taken from the deep electrode and the second is from electrode number 7, which is located on the frontal lobe. The τ^* value < 0.02 which corresponds to a first mode interaction. In **b**, same as a, where the second signal is obtained from electrode number 2 which records the M1 motor cortex. Here, $\tau^* = 0.03$ which corresponds to a second mode interaction.

Modes analysis. Next, we observed a bi-modal distribution of τ^* (See Fig. 4, b), supporting the hypothesis of the existence of two transfer mechanisms. The first one, dominated by τ^* centered around zero time lag, indicating a volume conduction, and a second mode, with larger τ^* (typically 30 milliseconds) could be related to information transfer through synaptic inputs. As shown above, every significant link is composed of several consecutive sub-links of 2.5 seconds each. To test the above hypothesis of the existence of two modes we will test next if all or at least most of sub-links belong to the same mode or if we have a random mixture of modes. If the links are mainly unique

that is almost all sub-links in a specific link have the same τ^* , as indeed found here, it supports the hypothesis of two modes. To this end, we examined the links sequences compositions, i.e., the sub-links, by dividing the τ^* range in Fig. 4 b into two regimes by the interception points of two fitted Gaussians, which we denote by '1' if τ^* of the window belongs to the first regime τ^* , and '2' if it falls in the second regime τ^* .

Then, for each sequence, we find the sequence composition of sub-links. For example, a sequence of 3 sub-links, may result in the composition '1,1,2', meaning that the first and second windows had τ^* 's from the first mode, and third window had τ^* in the second mode regime, as illustrated on Fig. 6. Interestingly, we find that for most of the sequences, the whole sequence was composed by either consecutive '1' or consecutive '2'. Meaning, that every interaction is of one type, and dominated by one transfer mechanism. We assume that the first mode, which consists of $\tau^* \sim 0$, are interactions that occur due to volume conduction process, and that the second mode of $\tau^* \sim 0.02$ represent information flow. It can be seen that only a very small fraction of the sequences are composed of mixed modes of 1's and 2's, (e.g., '1,2,1'). The results are summarized in Fig. 6.

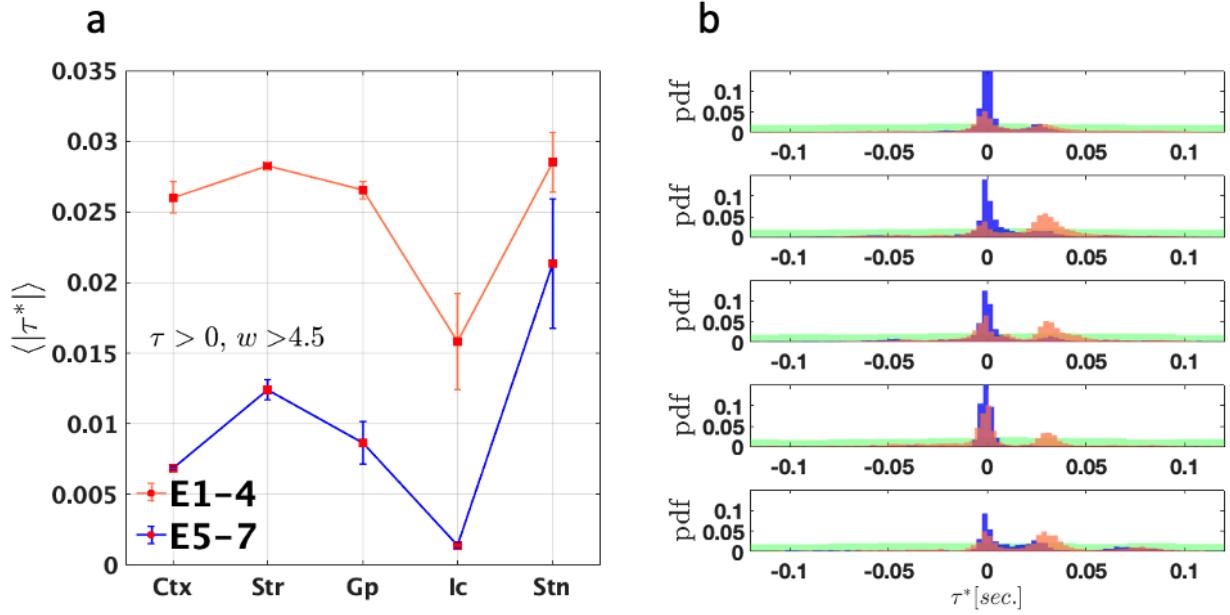


Figure 4: **Basal ganglia- cerebral cortex, average time delay results.** (a) Average $|\tau^*|$'s of nuclei, of interactions with $\tau > 0$. We show the mean time delays of the two signals of the electrodes sets, i.e., between E1-4, E5-7, and the moving electrode. $\tau > 0$ corresponds to the case in which the signal initiated (or earlier) at the cortex. This consist 80% of the real links. Note that the electrodes located at M1 (E1-4) have systematic, for all nuclei larger time delays, than the frontal lobe electrodes (E5-7) with a similar profile. (b) The distribution of τ^* for all cerebral cortex-BG nuclei Note that the distributions are bi-modal, suggesting two types of links. In light green, we present results of surrogate [25] data, where the deep electrode is taken form the nucleus, and the cortical electrodes are taken from different time of recording. Surrogate τ^* shows a uniform distribution without particular clustering behavior at specific τ^* as expected (light green). These results suggests that the mechanisms of volume conductance and information transfer occur. The number of time windows that were analyzed per nuclei appear on the top left box of each nuclei.

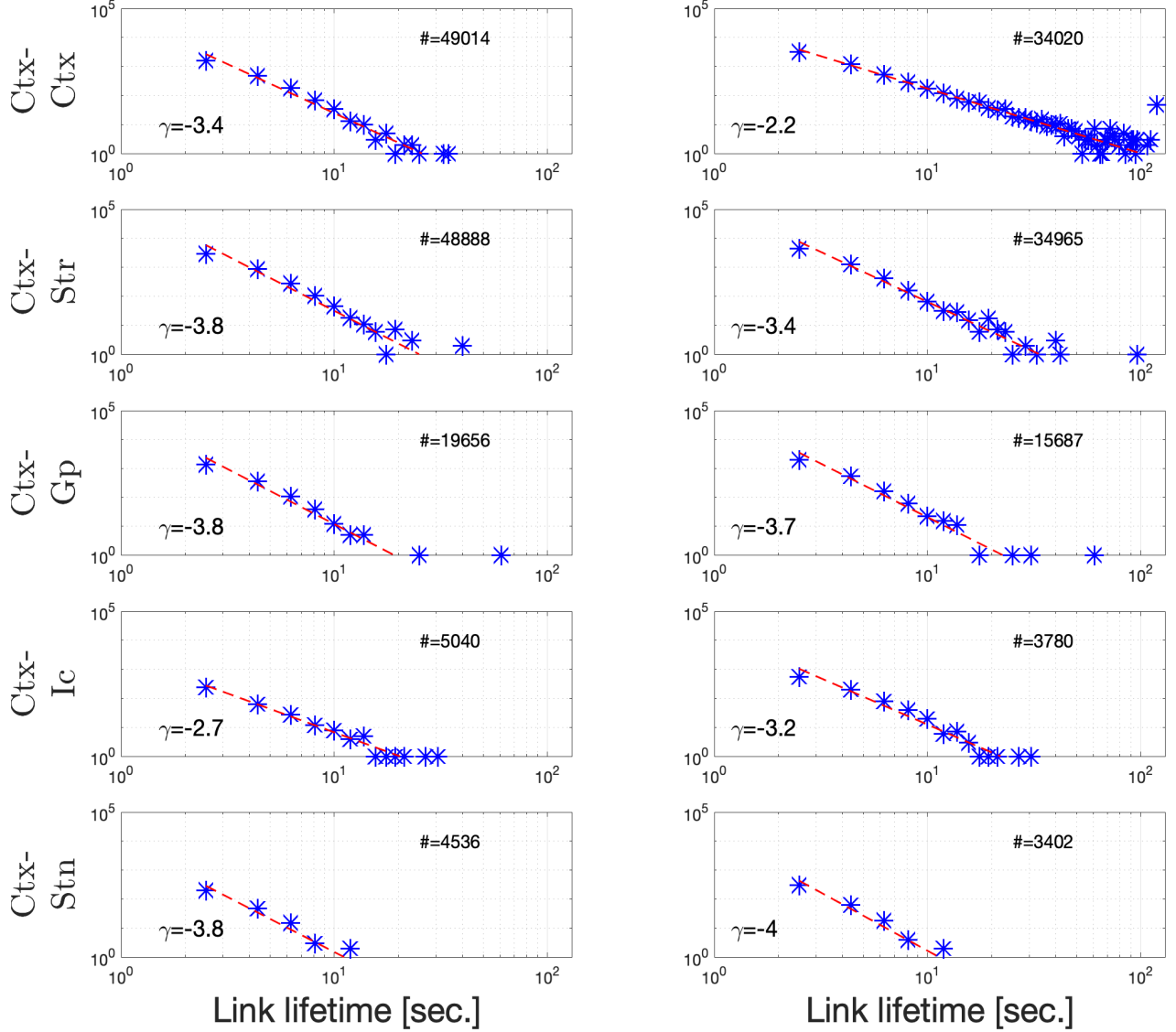


Figure 5: **Distribution of links duration of different nuclei.** Left and right columns show PDFs of links duration of E1-4 and E5-7 electrode sets respectively. Each site record (120 sec.), is divided in to 2.5 seconds long overlapping windows, with 25% overlap (0.625 seconds). Then, we analyze the cross-correlation within each time window segment between signals in the deep electrode and its matching time record of the electrode in the cortex, and w is calculated. If $w > 4.5$, we assume that the link is real. We then find the duration of the consecutive real links that were formed with the cortex electrodes at all sites of record. The results presented in log-log scale, suggest a power law distribution behavior (exponent γ is shown), and declination of real links duration as the nuclei is deeper, is visible. Note also, that for most nuclei links lengths are longer for the E5-7 frontal lobe electrode set compared to E1-4 motor M1 set. This suggests that distance affects LFP signals. Exponents show consistent increase with depth, except Ic, which consists of white matter in which signals might propagate more rapidly.

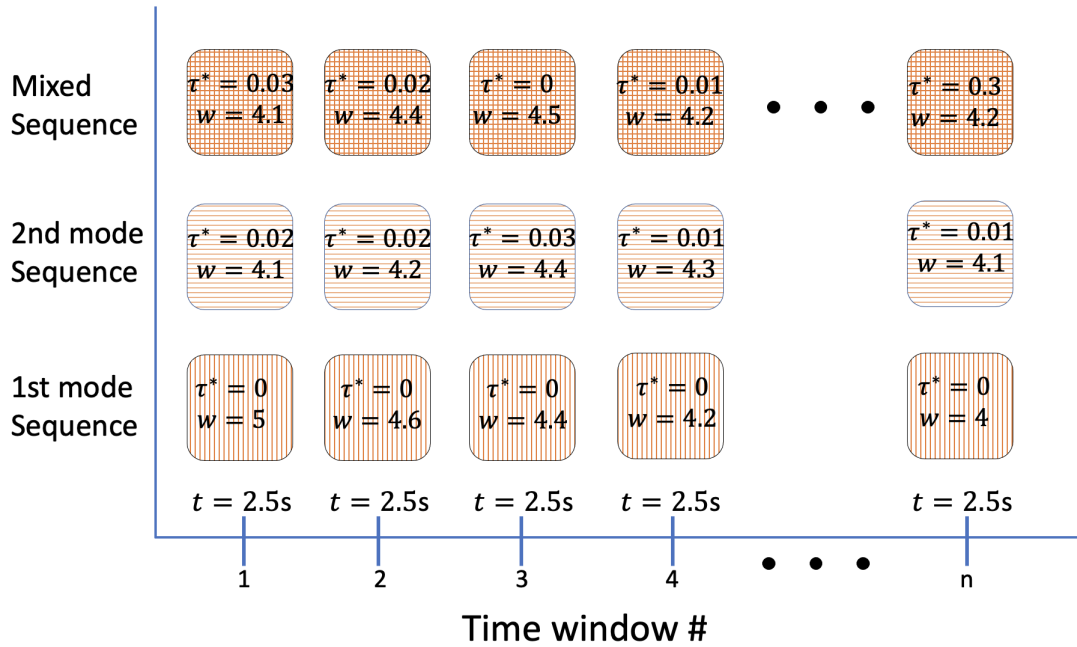


Figure 6: **Illustration of the first, the second and the mixed modes sequences composition.** This figure comprise of three rows. The bottom row represents a 1st mode sequence of length n . Note that for this sequence $\tau^* = 0$ for all windows. A sequence is n time-windows of which each time window had $w > 4$. Each sequence of length n , consists of n time windows that were cross-correlated. We calculate the τ^* of each of the n time windows, and ask what is the composition of those τ^* 's, i.e, to what mode this window belongs.

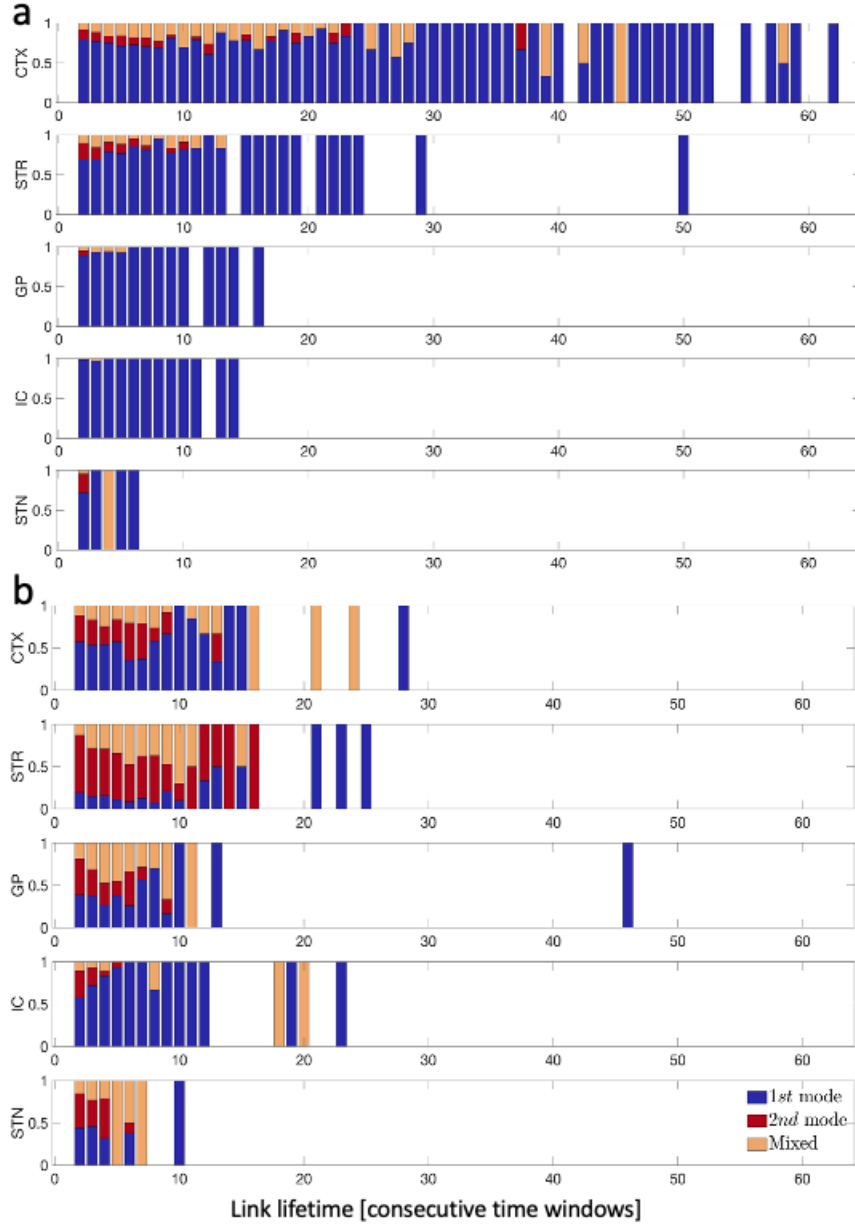


Figure 7: **Sequences modes composition**, $w > 4.5$. **(a)** analysis of compositions of links obtained between frontal cortex electrodes and the deep electrode. **(b)**: same as top, for the M1 electrodes. For each link of time length L , we analyze its sub-links τ^* values, and test whether they are in the ranges of the first or second modes. We find, that for most of the sequences, the sequence belongs to the the 1st or 2nd modes exclusively, while few of the sequences contains a mix of the both modes. If the whole sequence contains only τ^* values from the first (second) mode, we say that this sequence is a "first (second) mode" sequence. If the sequence contains combinations of first and second modes, we say it is a "mixed" sequence. Note that the frontal cortex links are dominated by first mode sequences $\langle \tau \rangle \simeq 0$, while second mode sequences $\langle \tau \rangle \simeq 0.02$ appear much more in the M1 links. Also note, that for the internal capsule (Ic) which consists of white matter, most links are from first mode in both frontal cortex and M1.

4. Summary and discussion

In this work, We tested the open question whether the LFP signals is a volume conductance phenomena or a synaptic input which represents information transfer. To address this question we develop a significance based cross correlation method and define a continuous time delayed link patterns. We performed simultaneous recordings of local field potentials (LFP) in the range of [0.1, 6000] Hz by 7 micro-electrodes which have been fixed on the 5th layer in the cerebral cortex and we used one micro-electrode to record sites while moving towards the BG nuclei. Each site was $200\mu\text{m}$ deeper than the previous one, and was aimed towards the BG. This procedure was done since the entering of the deep electrode to the frontal lobe cortex until it reached to the subthalamic nucleus. See illustration in Fig. 1(a). After data were collected and digitized, power spectrum densities were computed using Welch's power spectral density estimate method (Fig. 1(c)). Since the frequency range that was recorded includes the local field potential and the single and multi-unit activity, we apply low-pass filter to the signals in the range of [0.1, 80] Hz in order to get the field potentials. We split the 120 second duration of the recording at each site to 2.5 second windows with 0.5 seconds overlap between each window, and compute the cross correlation between each recording signal of the deep electrode with its matching time window from the seven cerebral cortex. Next, we developed a significance weight method to distinguish between spurious and real links. By applying this to a surrogate control data, we found a threshold score that enables us to assign for each link a weight which corresponds to its strength, and we compared the weights distribution to that of the surrogate signals in order to identify the real links. After removing the spurious interactions, we also find the time delay τ^* for each real link using the peaks in the shifting cross correlations. When plotting the average τ^* for both M1 and cortex frontal - lobe for each nuclei, we see (Fig. 4) that frontal-cortex areas yield shorter τ^* . Moreover, frontal-cortex area also produce more significant interactions, which can be seen in their weight scores (Fig. 2(g)).

When we compared real links duration from M1 and the cortex, we observed that as the recorded nuclei is deeper, links durations become shorter, and links of the deep electrode-cortex are longer than their corresponding deep electrode-M1, see Fig. 5. Furthermore, when looking at the τ^* distributions, we surprisingly observe two main modes, see Fig. 4(b). One, characterized by a short time delays ($\tau^* \sim 0$), and the second, with longer time delays ($\tau^* \sim 0.02$). We hypothesize, that these two modes are related to two different mechanisms of interaction, volume conductance (short τ^* , 1st mode) and threshold phenomena as synaptic inputs - an information transfer (longer τ^* , 2nd mode).

Our next question was to test whether a long term interaction, e.g. link, is mainly characterized by a τ^* sequence that belongs to one of the two modes. Interestingly, we find that most of the links consist of mainly 1st or 2nd mode only, and very few are a mix of the two, see Fig. 7. Frontal cortex - deep electrode links comprise mostly of 1st mode sequences, while 2nd mode sequences are more prevalent in the M1 - deep electrode links.

The significance of our method and results is that it may provide a framework to distinguish between volume conduction interactions, and real information flow, which currently an unsolved question. Future work may use tools from information theory and test whether links that belong to the second mode, conveys more information compared to those of volume conductance.

References

- [1] György Buzsáki, Costas A Anastassiou, and Christof Koch. The origin of extracellular fields and currents—eeg, ecog, lfp and spikes. *Nature reviews neuroscience*, 13(6):407–420, 2012.
- [2] Klaus Wimmer, Marc Ramon, Tatiana Pasternak, and Albert Compte. Transitions between multiband oscillatory patterns characterize memory-guided perceptual decisions in prefrontal circuits. *Journal of Neuroscience*, 36(2):489–505, 2016.
- [3] Alik S Widge, Sarah R Heilbronner, and Benjamin Y Hayden. Prefrontal cortex and cognitive control: new insights from human electrophysiology. *F1000Research*, 8, 2019.
- [4] J Andrew Henrie and Robert Shapley. Lfp power spectra in v1 cortex: the graded effect of stimulus contrast. *Journal of neurophysiology*, 94(1):479–490, 2005.
- [5] Conrado A Bosman, Jan-Mathijs Schoffelen, Nicolas Brunet, Robert Oostenveld, Andre M Bastos, Thilo Womelsdorf, Birthe Rubehn, Thomas Stieglitz, Peter De Weerd, and Pascal Fries. Attentional stimulus selection through selective synchronization between monkey visual areas. *Neuron*, 75(5):875–888, 2012.
- [6] James E Carmichael, Jimmie M Gmaz, and Matthijs AA van der Meer. Gamma oscillations in the rat ventral striatum originate in the piriform cortex. *Journal of Neuroscience*, 37(33):7962–7974, 2017.
- [7] Andrew Jackson and Thomas M Hall. Decoding local field potentials for neural interfaces. *IEEE Transactions on Neural Systems and Rehabilitation Engineering*, 25(10):1705–1714, 2016.
- [8] Klaus-Robert Müller, Michael Tangermann, Guido Dornhege, Matthias Krauledat, Gabriel Curio, and Benjamin Blankertz. Machine learning for real-time single-trial eeg-analysis: from brain–computer interfacing to mental state monitoring. *Journal of neuroscience methods*, 167(1):82–90, 2008.
- [9] JF Marsden, P Limousin-Dowsey, P Ashby, P Pollak, and P Brown. Subthalamic nucleus, sensorimotor cortex and muscle interrelationships in parkinson’s disease. *Brain*, 124(2):378–388, 2001.
- [10] John P Donoghue, Jerome N Sanes, Nicholas G Hatsopoulos, and Gyongyi Gaal. Neural discharge and local field potential oscillations in primate motor cortex during voluntary movements. *Journal of neurophysiology*, 79(1):159–173, 1998.
- [11] Maria C Rodriguez-Oroz, Manuel Rodriguez, Jorge Guridi, Klaus Mewes, Vijay Chockkman, Jerrold Vitek, Mahlon R DeLong, and Jose A Obeso. The subthalamic nucleus in parkinson’s

- disease: somatotopic organization and physiological characteristics. *Brain*, 124(9):1777–1790, 2001.
- [12] Shay Moshel, Reuben Ruby Shamir, Aeyal Raz, Fernando Ramirez de Noriega, Renana Eitan, Hagai Bergman, and Zvi Israel. Subthalamic nucleus long-range synchronization—an independent hallmark of human parkinson’s disease. *Frontiers in systems neuroscience*, 7: 79, 2013.
- [13] Maya Slovik, Boris Rosin, Shay Moshel, Rea Mitelman, Eitan Schechtman, Renana Eitan, Aeyal Raz, and Hagai Bergman. Ketamine induced converged synchronous gamma oscillations in the cortico-basal ganglia network of nonhuman primates. *Journal of neurophysiology*, 118(2):917–931, 2017.
- [14] SF Danish, JT Moyer, LH Finkel, GH Baltuch, JL Jaggi, A Priori, and G Foffani. High-frequency oscillations (≈ 200 hz) in the human non-parkinsonian subthalamic nucleus. *Brain research bulletin*, 74(1-3):84–90, 2007.
- [15] Shlomit Yuval-Greenberg, Orr Tomer, Alon S Keren, Israel Nelken, and Leon Y Deouell. Transient induced gamma-band response in eeg as a manifestation of miniature saccades. *Neuron*, 58(3):429–441, 2008.
- [16] Peter Brown and David Williams. Basal ganglia local field potential activity: character and functional significance in the human. *Clinical neurophysiology*, 116(11):2510–2519, 2005.
- [17] Constance Hammond, Hagai Bergman, and Peter Brown. Pathological synchronization in parkinson’s disease: networks, models and treatments. *Trends in neurosciences*, 30(7):357–364, 2007.
- [18] Tolga Esat Özkurt, Markus Butz, Melanie Homburger, Saskia Elben, Jan Vesper, Lars Wojtecki, and Alfons Schnitzler. High frequency oscillations in the subthalamic nucleus: a neurophysiological marker of the motor state in parkinson’s disease. *Experimental neurology*, 229(2):324–331, 2011.
- [19] Andrei Belitski, Stefano Panzeri, Cesare Magri, Nikos K Logothetis, and Christoph Kayser. Sensory information in local field potentials and spikes from visual and auditory cortices: time scales and frequency bands. *Journal of computational neuroscience*, 29(3):533–545, 2010.
- [20] Wen-Ju Pan, Garth Thompson, Matthew Magnuson, Waqas Majeed, Dieter Jaeger, and Shella Keilholz. Broadband local field potentials correlate with spontaneous fluctuations in functional magnetic resonance imaging signals in the rat somatosensory cortex under isoflurane anesthesia. *Brain connectivity*, 1(2):119–131, 2011.
- [21] Dora Hermes, Mai Nguyen, and Jonathan Winawer. Neuronal synchrony and the relation between the blood-oxygen-level dependent response and the local field potential. *PLoS biology*, 15(7):e2001461, 2017.
- [22] Ana Parabucki and Ilan Lampl. Volume conduction coupling of whisker-evoked cortical lfp in the mouse olfactory bulb. *Cell reports*, 21(4):919–925, 2017.

- [23] Honghui Zhang, Andrew J Watrous, Ansh Patel, and Joshua Jacobs. Theta and alpha oscillations are traveling waves in the human neocortex. *Neuron*, 98(6):1269–1281, 2018.
- [24] Tatsuo K Sato, Ian Nauhaus, and Matteo Carandini. Traveling waves in visual cortex. *Neuron*, 75(2):218–229, 2012.
- [25] Gemma Lancaster, Dmytro Iatsenko, Aleksandra Pidde, Valentina Ticcinelli, and Aneta Stefanovska. Surrogate data for hypothesis testing of physical systems. *Physics Reports*, 748:1–60, 2018.

Supporting information

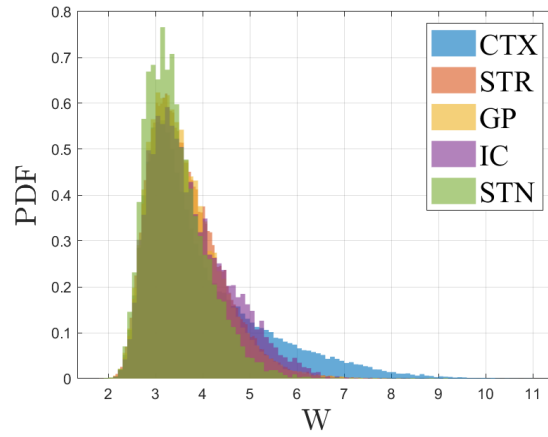


Figure 8: Note that Ctx-Ctx interactions (blue) yield higher w 's. Deeper Stn-Ctx (green) interaction yield the lowest w distribution, while Str-Gp-Ic w distributions increase gradually in between.

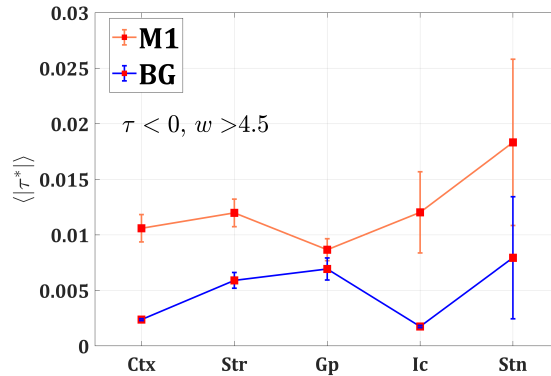


Figure 9: **Average time delay results for nuclei.** (a) Average $|\tau^*|$'s of nuclei, of interactions in which $\tau < 0$. We show the time delays of the two electrodes sets, M1 and E5-7. $\tau < 0$ corresponds to the case in which the interaction initiated in the basal ganglia. Similar to the results that are shown in Fig.4(b) M1 electrodes have a larger time delays, than the E5-7 with a similar profile. This holds for all nuclei.

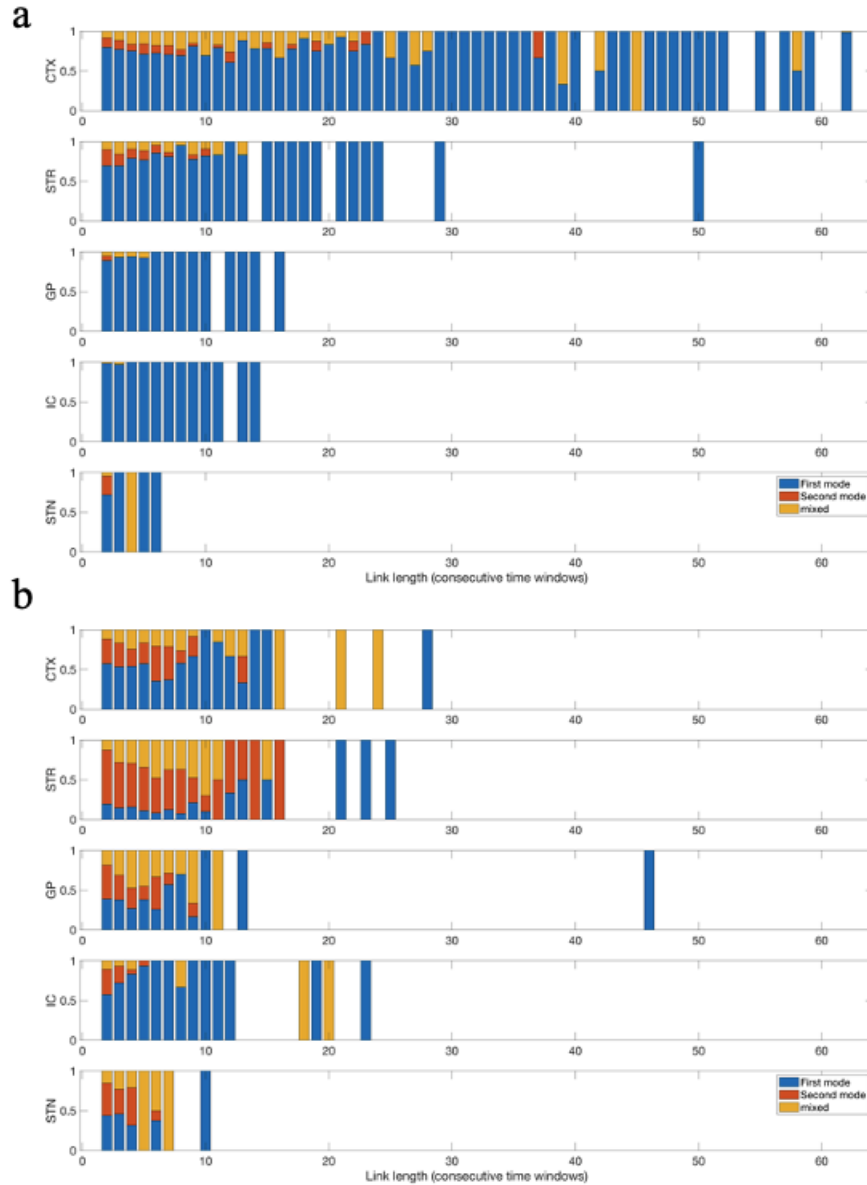


Figure 10: **Sequences modes composition**, $w > 4$. **(a)** analysis of compositions of links obtained between M1 electrodes and the deep electrode. **(b)**: same as top, for the frontal cortex electrodes. For each link of time length L , we analyze its sub-links τ^* values, and test whether they are in the ranges of the first or second modes. We find, that for most of the sequences, the sequence belongs to the 1st or 2nd modes exclusively, while few of the sequences contains a mix of the both modes. If the whole sequence contains only τ^* values from the first (second) mode, we say that this sequence is a "first (second) mode" sequence. If the sequence contains combinations of first and second modes, we say it is a "mixed" sequence. Note that the frontal cortex links are dominated by first mode sequences, while second mode sequences appear much more in the M1 links. Also note, that for the internal capsule (Ic) which consists of white matter, most links are from first mode in both frontal cortex and M1.

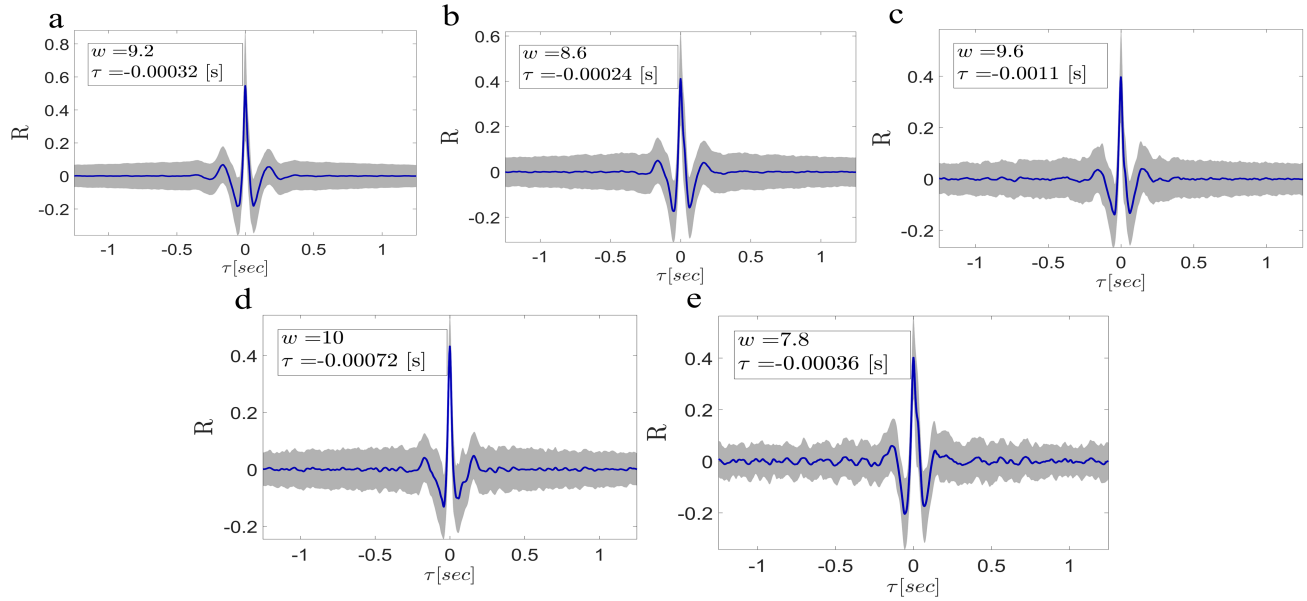


Figure 11: **Cross-correlations.** The cross-correlations of the E5-7 (on the cortex) electrodes with the deep electrode, while being in the five nuclei. (a-e) show the cross-correlations between E5-7-Ctx, E5-7-Str, E5-7-Gp, E5-7-Ic and E5-7-Stn respectively. Here we show only cross-correlations with $w > 4.5$ and $\tau^* < 0.05$ ms, of the time windows that were analyzed. In blue is the mean, and the shaded area represents the standard deviation. Shown here are results of E5-7 electrodes interaction. (See SI for results of E1-4 electrodes.)